Exploration Geophysics

ISSN: 0812-3985 (Print) 1834-7533 (Online) Journal homepage: https://www.tandfonline.com/loi/texg20

On-time modelling using system response convolution for improved shallow resolution of the subsurface in airborne TEM

Esben Auken, Nikolaj Foged, Kristoffer Rønne Andersen, Nicklas S. Nyboe & Anders Vest Christiansen

EXPLORATION GEOPHYSICS
https://doi.org/10.1080/08123985.2019.1662292

On-time modelling using system response convolution for improved shallow resolution of the subsurface in airborne TEM

Esben Auken [a], Nikolaj Foged [a], Kristoffer Rønne Andersen [a], Nicklas S. Nyboe [b] and Anders Vest Christiansen [a]

[a]Department of Geoscience, WATEC, Aarhus University, Aarhus, Denmark; [b]SkyTEM Surveys, Aarhus, Denmark

ABSTRACT

We describe a new approach for modelling airborne transient electromagnetic (TEM) data which combines the use of on- and off-time data for inversion. Specifically, the response is modelled using system response convolution both during and after transmitter ramp-down. High near-surface sensitivity can be achieved through a combination of fast transmitter ramp-down, broad receiver system bandwidth, efficient suppression or explanation of the primary field, and by combining the use of on-time gates with accurate knowledge of the system response. The system response can either be calculated based on the transfer function of the individual system components (i.e. receiver coil, amplifiers, low-pass filters and current waveform) or it can be measured at high altitude. The latter approach has the advantage of avoiding the specific modelling of individual system components. By comparing model parameter uncertainty when the on-time gates are included in the inversion versus when they are not, we show that a significant improvement in near-surface sensitivity is obtained. The method is used to invert both synthetic and field data. In the inversion of synthetic data, we see clear improvements in the determination of thin shallow layers, especially when they are resistive. This is confirmed by inversion of field data where we observe more pronounced structures with better definition of layer boundaries and layer resistivities.

ARTICLE HISTORY
Received 2 October 2018
Accepted 4 June 2019

KEYWORDS
Airborne survey; airborne electromagnetics; airborne geophysics; time-domain

Introduction

The limits of transient electromagnetic (TEM) systems are constantly being pushed by manufacturers and modellers to achieve a better sensitivity to both near-surface and deep geological targets. Deep targets are resolved mainly by increasing the transmitter moment (Spies 1989) and decreasing the noise due to, for example, system vibrations (Macnae and Milkereit 2007), whereas completely different measures are needed to improve the model parameter estimation of the near-surface. A review on recent developments in airborne EM can be found in Everett (2012) and Auken, Boesen, and Christiansen (2017).

In TEM, the near-surface is probed with the time gates close to the termination of the current pulse. The current ramp-down is not instantaneous, but depends on the transmitter technology and the size of the magnetic moment, meaning that it may be anywhere from a few microseconds to more than a millisecond. For near-surface resolution, a very short ramp-down is optimal. Time gates measured during the current ramp-down (referred to as on-time gates in this paper) may also increase the near-surface resolution, but special care is needed if one wants to measure the Earth response during the current ramp-down, where the primary field is non-zero. In airborne TEM, the primary field is generally orders of magnitude larger than the secondary field from the Earth and it is therefore challenging to isolate the secondary field part of measurements made during ramp-down.

Different methods have been proposed to remove the primary field during ramp-down. Use of a bucking coil is one way to reduce the primary field, but in general this approach is unstable due to geometrical variations during flight. Also, the bucking efficiency is frequency dependent, which tends to reduce bucking efficiency close to rapid changes in the transmitted current. Examples of systems using bucking coils are AeroTEM (Balch, Boyko, and Paterson 2007) and VTEM (Legault et al. 2012; Witherly, Irvine, and Morrison 2004). Another strategy is to position the receiver coil in a so-called zero-position, where the net flux of the primary field through the receiver is zero (Kirkegaard et al. 2012; Schamper, Auken, and Sørensen 2014). This passive method reduces the primary field by orders of magnitude compared with a central-loop system. However, it requires a very rigid coil setup, and even small changes in the geometry will introduce some primary field flux through the receiver coil. Such small variations in geometry occur constantly for airborne systems and a small residual primary field therefore remains in the measured signal. This residual primary field needs to be

CONTACT Nikolaj Foged nikolaj.foged@geo.au.dk Department of Geoscience, Aarhus University, C.F. Mollers Alle 4, DK-8000 Aarhus C, Denmark

removed to isolate the secondary field. A more general technique is to estimate the primary field and subtract it from the measured signal. This has been done by Lane et al. (2000), Smith (2001), and Schamper, Auken, and Sørensen (2014), and requires detailed information about the system geometry and transmitted current.

Lastly, there are methods that aim at describing or measuring the actual system response (SR) and in this way taking all effects into account regardless of their origin. The SR is defined as the combined convolution of the impulse responses of the individual system components (i.e. receiver coil, amplifiers and low-pass filters) and the time derivative of the current waveform. The SR method is general and can be used to calculate the forward response from any AEM system with a known SR. A simple SR convolution was outlined in a conference proceeding by Yin et al. (2008) and also discussed in Raiche (1998).

In this article, we describe the implementation of a forward algorithm where the impulse responses of all the system components are convolved with the step response (B-field) of a layered Earth. As the convolution is done in the forward domain rather than on the data, it is a stable process, where the decay curve can be calculated at all times. We compare the measured SR to a theoretical SR calculated from the individual system components (receiver coil, receiver, current waveform), and perform a validation at the Danish TEM test-site (Foged et al. 2013). Finally, we demonstrate the increased resolution capability of an AEM system using on-time gates compared with a system in which these gates are omitted (which is the normal case) through synthetic and field data examples.

Data presented here are measured with the SkyTEM system (Sørensen and Auken 2004), which uses zero-positioning in combination with the primary field compensation (PFC) technique (Efferso 2014) to remove the primary field influence during ramp-down. The PFC technique removes the remnant primary field measured by the receiver (K. I. Sørensen, personal communication), which is necessary for our SR inversion of data during ramp-down where we assume that the data are primary field free. Derivation of the SR is based on an analysis of measurements taken at high altitude (Andersen et al. 2015; Nyboe and Mai 2017). The PFC and SR calculation techniques are proprietary to SkyTEM Surveys ApS, and their implementations are not available in further detail.

Modelling: convolution with the system response

The TEM signal recorded during transmitter ramp-down generally consists of two contributions: the primary field from the transmitter and the secondary field from the Earth. This is shown schematically in Figure 1 for a short, exponential type, current decay. If the primary

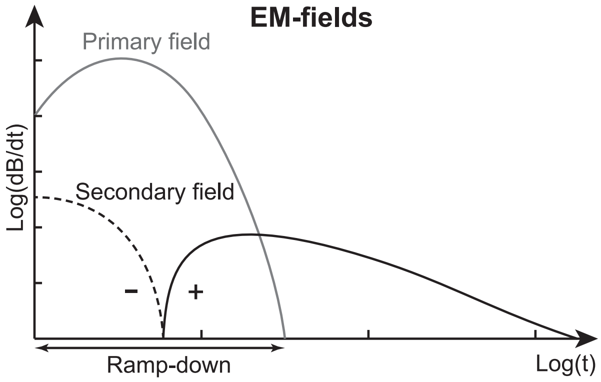

Figure 1. A schematic drawing of a measurement during and after ramp-down, where $t = 0$ is defined as the start of the ramp-down. During ramp-down, the primary field (grey line) is generally orders of magnitude larger than the secondary field (black line). After ramp-down, the primary field is zero and only the secondary field component is there. Dashed line indicates negative secondary field.

field contribution can be effectively suppressed or subtracted, only the desired secondary field remains, which typically includes a sign change in the first part of ramp-down interval, as indicated in Figure 1.

In the following, we assume that we only measure the secondary response from the ground and no primary field from the transmitter. When modelling the very early time response explicitly, a full and accurate description of the system is needed because these data will be heavily influenced by the SR. The main components of the SR are the transmitter waveform and the filter characteristics of the receiver coil and the electronics. The latter two can typically be modelled as ideal low-pass filters of appropriate order, while the waveform can be measured accurately using a current sensor with sufficient bandwidth and sensitivity (or a combination of current sensors with complimentary bandwidths and sensitivities, if necessary). An alternative to such an explicit description is to measure the full SR at a high altitude where the secondary field from the ground is negligible. Ideally, the measured SR is a convolution of the above-mentioned effects and any other effect present in the system, which might be poorly known to us. Such effects can be minor time shifts of the gates with respect to the transmitted waveform due to signal transmission delays in cables and microprocessors.

A TEM system measures the induced electromotive force in the receiver coil, which is proportional to the time derivative of the flux through the coil and therefore proportional to the time derivative of the ambient magnetic field. We denote the measured voltage by V_{meas} which is a convolution of the time derivative of the theoretical magnetic field from a current step turn-off, B_{step}, the time derivative of the transmitter current, $I(t)$, and the system filters, h_{system} (receiver coil and electronics). B_{step} contains only the secondary field from the ground and no primary field. We assume that the measurements are primary field free, unbiased, and noise free, and get.

$$V_{meas} = NA\frac{dB_{step}}{dt}*\frac{dI}{dt}*h_{system}, \quad (1)$$

where A is the receiver coil area and N is the number of turns in the receiver coil. If we gather the waveform and the filters into a system response, SR.

$$SR = \frac{dI}{dt}*h_{system}, \quad (2)$$

and we get

$$V_{meas} = NA\,\frac{dB_{step}}{dt}*SR = NAB_{step}*\frac{dSR}{dt}. \quad (3)$$

For actual calculations of V_{meas}, dSR/dt is given by

$$\frac{dSR}{dt} = SR' = \frac{d^2I}{dt^2}*h_{system}. \quad (4)$$

The implementation of the convolution is performed as a sum of analytically evaluated integrals so that

$$B_{step}*SR'(t) = \sum_{ij}\int F_i(B_{step}, s)G_j(SR', t-s)ds. \quad (5)$$

F_i and G_j are interpolation functions that are used to calculate the value of the discretely sampled B_{step} and SR' at all other times. We use natural cubic splines (Forsythe, Malcolm, and Moler 1977) for F_i and let G_j be a simple linear interpolation. SR' is assumed to be provided with a fine sampling and a linear interpolation is therefore sufficiently accurate. B_{step} is known at times $t_i^F, i \in \{1,\ldots,N\}$ with values B_i. The splining process generates constants a_i^F, b_i^F, c_i^F and d_i^F for each interval $[t_i^F, t_{i+1}^F]$ so

$$F_i(B_{step}, t) = a_i^F(t-t_i^F)^3 + b_i^F(t-t_i^F)^2 + c_i^F(t-t_i^F) + d_i^F, \quad (6)$$

where $t_i^F \le t \le t_{i+1}^F$. Similarly, for the system response one has

$$G_j(SR', t) = a_j^G(t-t_j^G) + b_j^G, \quad t_j^G \le t \le t_{j+1}^G. \quad (7)$$

In this form, one can analytically calculate the integral for every time interval where the splines are valid. That is

$$\int_{\max(t_i, t-t_{j+1})}^{\min(t_{i+1}, t-t_j)} F_i(B_{step}, s)G_j(SR', t-s)ds \quad (8)$$

can be calculated directly for all pairs of i and j. We sample the convolution (Equation 5) in an adaptive fashion between 6 and 96 equidistant logarithmically spaced points per decade as described in Appendix A.

Because the convolution is performed in the time-domain, the secondary field B_{step} has to be known from $t = 0$ and onwards. In the implementation, B_{step} is calculated for $t \ge 10^{-8}$s with a linear extrapolation to $t = 0$. To increase the calculation speed of B_{step} we have optimised implementation of the calculation using the Gaver–Stehfest method for the inverse Laplace transform (Knight and Raiche 1982) for the temporal integral and the Hankel transform (Johansen and Sørensen 1979) for the spatial integral. Our implementation benefits from a vectorised calculation of the reflection coefficients (Kirkegaard and Auken 2015). We furthermore adaptively sample B_{step} with 3–12 logarithmically spaced points per decade using the same algorithm as used for the convolution. The final accuracy of forward response, V_{meas}, is around 0.1%.

System response validation

In this section, we validate the SR and the SR-modelling by comparing: (1) the measured SR with a theoretical SR calculated from explicit measurements of ramps and filters of the same airborne TEM system; and (2) measured data, including on-time gates, from the TEM-test site with the test-site forward response modelled using the SR.

Validation of measured SkyTEM system responses

Currently, SR modelling is carried out for the low moment part of the SkyTEM data, because this is the moment predominantly probing the shallow part of the subsurface. The key low moment specifications of the two SkyTEM systems used in the examples are listed in Table 1.

The two low-pass filters of the SkyTEM 304 system and the convolution of the filters are shown in Figure 2(a) (h_{system}, red line). Note that h_{system} stretches out to around 5 µs with a peak around 1.5 µs, and the filters therefore delay the Earth impulse response by $\sim$ 1.5 µs and stretch it slightly. For gates before $\sim$ 20 µs, this has a very large effect and underlines the need to model everything extremely accurately. Details of the calculations can be found in Appendix B.

It is instructive to look at d^2I/dt^2, since the secondary response relates closely to the second time derivative of the waveform (Figure 2b). Within the first 1 µs, d^2I/dt^2 is negative, which corresponds to the start of the ramp-down. After 1 µs the curvature is positive and for $t > 2$ µs the curvature falls exponentially and is close to zero after 6 µs.

Table 1. Key system specifications for low moment for the SkyTEM 304 and 312 system.

Low-moment setup	SkyTEM 304	SkyTEM 312
Transmitter area per turn (m^2)	314	314
Transmitter turns	1	2
Transmitter-current (A)	$\sim$ 9	$\sim$ 5
Transmitter-peak moment (Am^2)	$\sim$ 3000	$\sim$ 3000
Turn-off time (µs)	$\sim$ 5	$\sim$ 23
Receiver coil low-pass filer	210 kHz, 2. order	210 kHz, 2. order
Receiver instrument low-pass filer	300 kHz, 1. order	300 kHz, 1. order

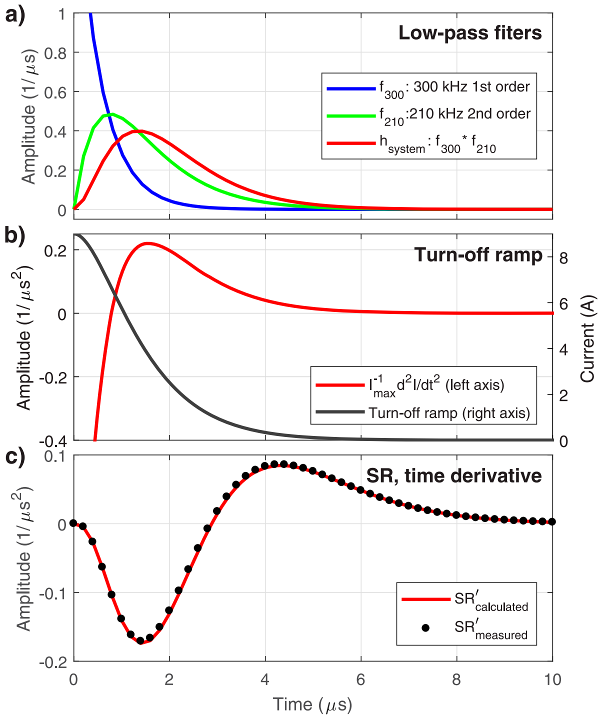

Figure 2. (a) Two low-pass filters (blue and green) and their convolution (h_{system}, red). (b) The turn-off part of the waveform is shown in grey and the second time derivative of the waveform normalised by the peak current I_{max} is shown in red. (c) The red line ($SR'_{calculated}$) is the resulting calculated time derivative of system response and the black dots mark the measured time derivative of the system response ($SR'_{measured}$) for the SkyTEM 304 system. Both SR' values are normalised by the peak current. The RMS fit of $SR'_{measured}$ to $SR'_{calculated}$ is 0.0011.

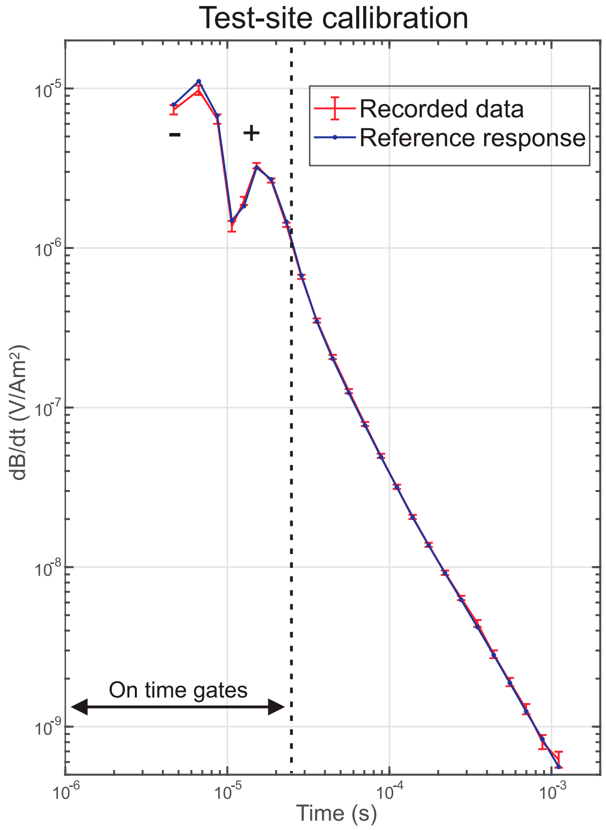

Figure 3. Test-site calibration plot for low-moment, SkyTEM 312 system. The match between the system-specific reference response (blue) and the recorded SkyTEM data at the Danish TEM test site from a height of ∼ 35m. The first four gates are negative.

As shown in Figure 2(c), the theoretical SR, calculated based on the two low-pass filters in Figure 2(a) and the waveform in Figure 2(b), agrees very well with the measured SR for the SkyTEM 304 system.

Test-site validation

Validation of the SR and the SR modelling scheme was also performed at the Danish TEM test-site, following the TEM test-site calibration scheme by Foged et al. (2013). The calibration/validation example in this section is for the SkyTEM 312 system, with the same system setup as for the later presented field example (detailed system specifications are given in the field example section). Focusing on the low moment, the sounding curve contains eight on-time gates in the time range 2–23 µs, as indicated in Figure 3. Figure 3 shows the system-specific reference response and the recorded low-moment SkyTEM data after calibration. A good match to the reference response is obtained for both on-time and off-time gates.

Improved model resolution by including on-time data

In this section, we demonstrate the model resolution enhancement by including the on-time gates, enabled via the SR-modelling scheme, for two synthetic examples and one field example.

Noise model

To investigate the effect of including on-time data via SR-modelling in a model sensitivity analysis, realistic data uncertainties, σ_{data}, need to be estimated.

The first part of the noise model is a 3% uniform uncertainty. Systematic uncertainties are hard to determine, but several factors play a role, such as transmitter current variations due to temperature changes, timing jitter and the accuracy of the PFC. To take this into account, we add an additional relative uncertainty, σ_{SR}, on the on-time data given by

$$\frac{\sigma_{SR}}{V_{data}} = 3\% \cdot \left(\frac{t}{10^{-5}}\right)^{-1}, \tag{9}$$

where V_{data} are forward modelled data. This contribution mainly increases the data uncertainty for times gates around the sign change and for the very early time gates ($t \leq 10$ µs) where the PFC and the SR plays a major role (see Figure 4).

Finally, the noise model also includes an absolute white noise contribution and a contribution due to man-made sources like VLF transmitters. These contributions are determined from noise measurements

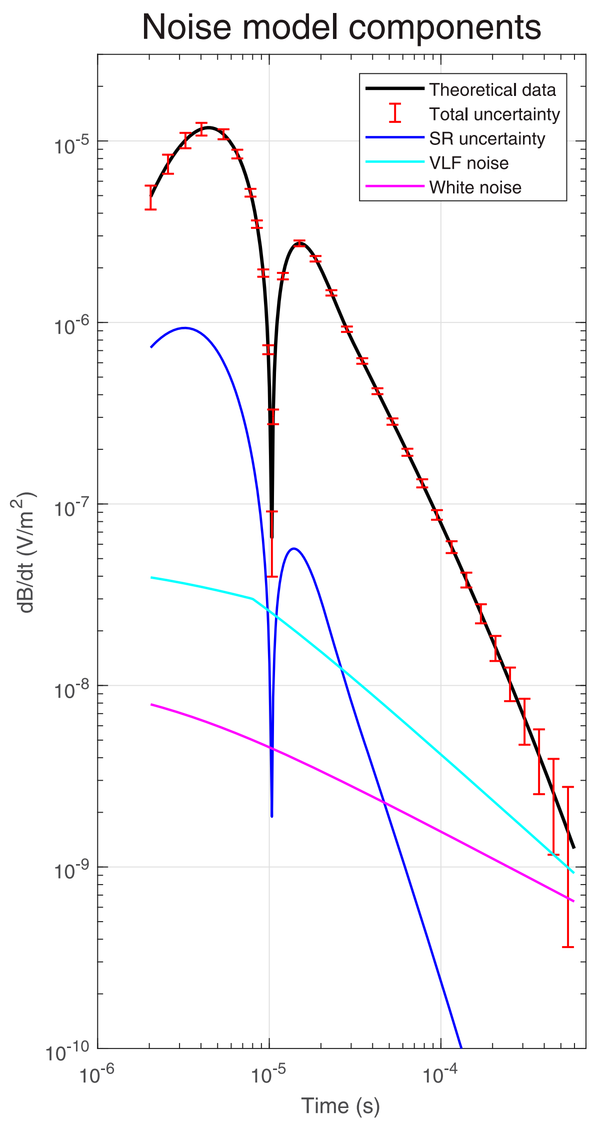

Figure 4. Noise model and theoretical data with total $\pm\sigma_{data}$ limits. Shown in absolute numbers, the magenta line is the background noise contribution, the cyan line is the VLF noise contribution, and the blue line is the contribution from the SR-uncertainty. Error bars represent the total uncertainty (including the 3% uniform contribution), for the theoretical response (black line).

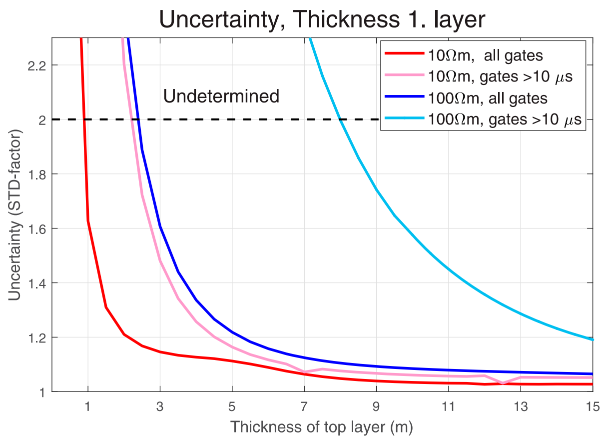

Figure 5. The standard deviation factor for the resistivity of a thin layer (1–15 m) with a resistivity of 10 Ωm (red curves) and 100 Ωm (blue curves) above a 20 Ωm background as a function of the thickness of the layer. The dark red and dark blue curves show the analysis with on-time gates, whereas the light red and light blue curves are the analyses without the on-time gates.

and are not important for the early time gates and are only included here for completeness. The noise model is shown in Figure 4, together with a forward response and the resulting $\pm\sigma_{data}$ limits. The uncertainty is dominated by the SR uncertainty at early times before $t \leq 10$ µs, then becomes dominated by the uniform uncertainty up to $t \leq 30$ µs and it is finally dominated by the background noise (white noise and VLF noise). For the field data, the combined VLF and background noise contribution is estimated from the stacking of the raw transients.

Estimating model parameter uncertainties

A direct way of investigating the model parameter resolution is to plot the model parameter standard deviation factor (STDF) obtained with and without the on-time gates. The STDF is determined from the a posteriori covariance matrix, which is given in the linearised approximation (Auken and Christiansen 2004; Tarantola and Valette 1982) as

$$C_{est} = (G^T C_{obs}^{-1} G)^{-1} \tag{10}$$

where G is the Jacobian of the forward data with respect to the model parameters and C_{obs} is the data covariance matrix. Standard deviations on the model parameters are given by the diagonal elements of C_{est} and because the model parameters are in log space, these elements become standard deviation factors. Therefore, under the assumption of a lognormal distribution and that the linearised approximation is sufficient, the $\pm\sigma$ limits for parameter m_i are given by

$$\frac{m_i}{STDF} < m_i < STDF \cdot m_i, \tag{11}$$

where $STDF = \exp\left(\sqrt{C_{est}(i,i)}\right)$.

To illustrate the improved determination of layer parameters by including the on-time data we plot the STDF (Figure 5) for the resistivity of a thin surface layer above a 20 Ωm background, simulating a SkyTEM system with a turn-off time of $\sim$ 10 µs. We set the resistivity of the top layer to 10 and 100 Ωm respectively and vary the thickness from 0.5 to 15 m.

For the 10/20 Ωm model (red curves in Figure 5) we see a clearly better determination of the top layer resistivity by including the on-time gates if the layer is thinner than $\sim$ 5 m. If we set the STDF limit to 1.2 for a well-determined parameter, we can resolve the top layer resistivity if the layer is thicker than $\sim$ 2m with on-time gates, whereas the layer needs to be thicker than $\sim$ 4.5m without the on-time gates. For the 100/20 Ωm model (blue curves in Figure 5), the improvement by including the on-time gates is even more significant. The top resistivity is well-determined for a layer thickness > 5 m for the on-time gates case, whereas the layer needs to be thicker than ~15 m to be well-determined without the on-time gates.

In conclusion, we see a significant improvement in parameter resolution by including the on-time gates even when we have taken the extra uncertainty of these data into account. The exact improvement will be system- and model dependent.

Inversion example, synthetic data

The STDF shown in Figure 5 shows a clear improvement in the determination of thin layers, however they are calculated for single soundings and do not include many effects that are present in actual inversions of AEM data. Here we show inversions of synthetic data calculated using the AarhusInv 1D code (Auken et al. 2015) for a 100 Ωm layer above a 20 Ωm background with a thickness varying from 0 to 10 m over a distance of 1000 m (Figure 6(a)). We generate synthetic sounding data for every 10 m and apply the noise model described previously. The synthetic dataset is then inverted with and without the on-time gates using a smooth model description with 30 layers starting at 0.5 m in the top layer. The layer thicknesses are log-spaced with the last layer boundary at 193 m. The inversion is carried out in a laterally constrained inversion (LCI) setup (Auken et al. 2005), with vertical constraints by a standard deviation factor of 2 and horizontal constraints by 1.3. To enhance layer boundaries, in the inversion model for this case of a strictly layered true model, we minimise the objective function using the L1 norm, which in such a case favours a sharp inversion result. The inversion results without and with the on-time gates are shown in Figure 6(b) and 6(c) and the top layer resistivity is also much closer to the true resistivity. Only when the top layer becomes very thin (< 2–3 m) is the resolution decreasing, but not to the same degree as for the result without the on-time gates.

Inversion example, real data

The field example is from a 2016 SkyTEM survey from Reynolds Creek, Idaho, USA, (HydroGeophysics Group 2017; Seyfried et al. 2018) and we focus on just one line of the 800 km survey. The SkyTEM system flown was a dual moment system (low-moment, high-moment) and the system response was determined for the low-moment part only. The zero position of the receiver coil together with the PFC method was used to remove the primary field prior to inversion. The survey was conducted with the SkyTEM 312 system, which uses 12 transmitter turns for the high-moment part and one turn for the low-moment part. The presence of the 12 transmitter turns results in a relative turn-off time at ~ 23 µs for the low-moment part. Using the on-time gates and the SR-modelling scheme enabled us to include eight on-time gates in the time range 2–23 µs for the low-moment part, while the first gate time is at ~ 25 µs for the inversion results without the on-time gates. Figure 7(d) and 7(e) shows a single sounding curve with and without the on-time gates.

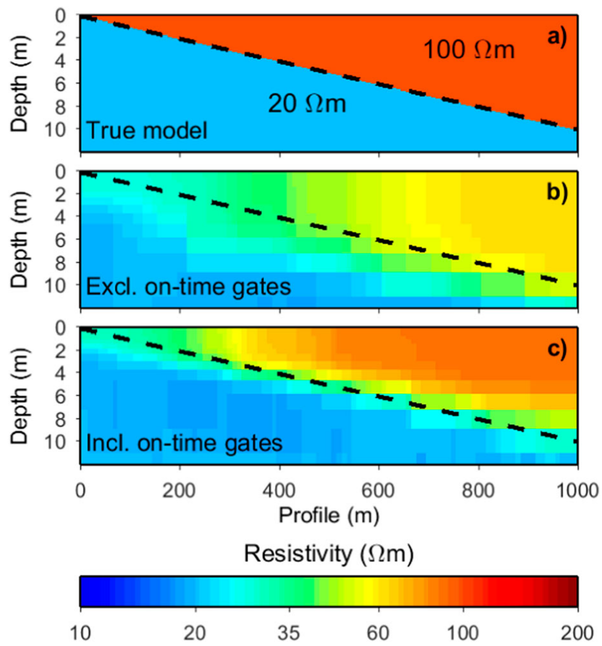

Figure 6. (a) The true model. (b) LCI, L1-norm inversions without on-time data (data from 10 µs). (c) LCI, L1-norm inversions with including on-time data.

An LCI with a smooth 30-layer model and a L2-norm regularisation scheme with the AarhusInv code was used. Figure 7(a) displays a 9-km long resistivity section of the selected flight line for the inversion with the on-time gates. To evaluate the effect of including the on-time gates in the inversion, Figure 7(b) (without on-time gates) and Figure 7(c) (with on-time gates) show close-ups of the upper 40 m of the resistivity section from the 3.5 km centre part of the section in Figure 7(a) (the interval between the two dashed lines). The vertical exaggeration is 12 and the sections are plotted on a depth scale for easier comparison. The inversion setup is identical for the two inversions and the two inversion results fit the data equally well.

Focusing on the 30–40 Ωm structure at mark I in Figure 7(b) and 7(c), it is clear that the structure is more well-defined and that the resistivity contrast is higher for the section including the on-time gates. This is also seen in Figure 7(f), where the models marked with an arrow in Figure 7(b) and 7(c) are plotted for the two inversions results. The two models in Figure 7(f) differ significantly in the top ~ 18 m and produce similar resistivities for the deeper model part. As seen in Figure 7(d) and 7(e), the data fits for the two models in Figure 7(f) are equally good. At mark II in Figure 7(b) and 7(c), we see a conductive structure, which is better defined and has another shape for the results including the on-time gates. At mark III, we again see an enhanced conductive structure by including the on-time gates.

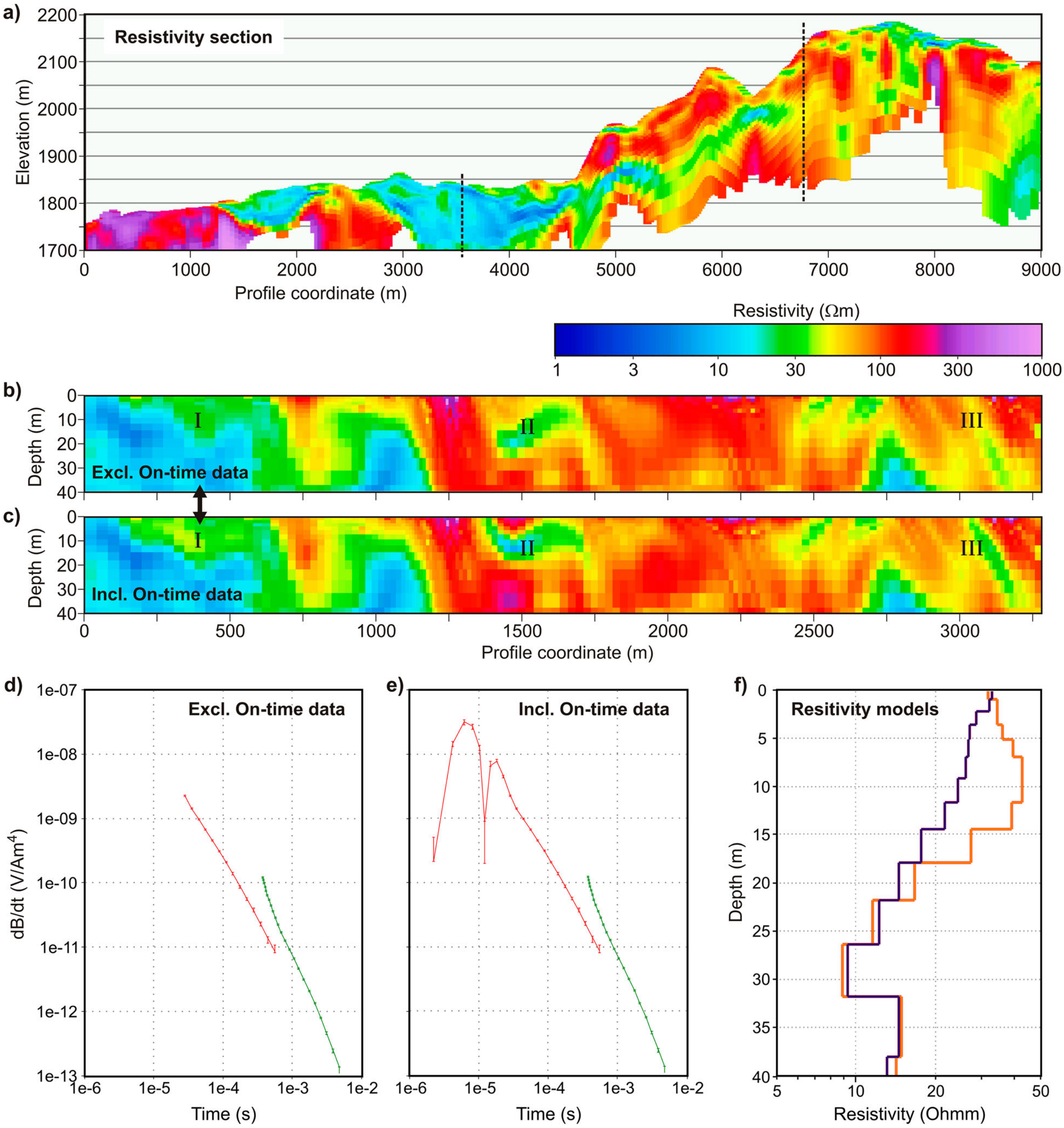

Figure 7. (a) Inversion result of one flight line including the on-time gates. (b,c) Top 40 m zoom-in on the interval between the dashed lines in (a) and plotted on a depth scale, (b) without the on-time gates and (c) including the on-time gates. (d,e) High (green) and low (red) moment sounding curves, with error bars marking the recorded data, while the line is the forward response from the models plotted in (f) and marked with the arrow in (b) and (c).

As expected, and as the synthetic examples showed, we get an enhanced resolution of the very shallow geological structures by including the on-time gates enabled by the SR-modelling scheme.

Discussion

Measurement of the SR has some advantages compared with calculating it from the different system components because a measured SR provides direct information on how the EM-signal is recorded by the instrumentation. Calculating the SR based on the current waveform, system low-pass filters, etc. introduces some uncertainty because the different components are known to only a certain degree of accuracy. In both cases, one needs to make sure that the SR is constant throughout a survey when modelling/inverting the data, which among other things, demands a constant current waveform.

The SR convolution modelling approach enables use of the on-time gates and gates just after the current ramp-down. The primary field needs to be removed prior to inversion, and the quality of the on-time gates therefore varies depending of the accuracy of the primary field removal. Detailed information regarding removal of the primary field is kept as proprietary information by the instrument manufacturers/surveying companies, and judging the quality and assigning valid data uncertainties for the on-time gates is therefore challenging.

The enhancement of the near-surface model resolution depends on the quality and number of the on-time gates. This actually means that a TEM-system with a relatively long turn-off time benefits most from including the on-time gates because more on-time gates are available.

The inversion model needs to reflect the enhanced very near-surface resolution provided by the on-time gates. This is done by adding a few more and thinner layers in the top of the inversion model. This leads to the question of whether the frequency content is now so high that the quasi-static approximation is challenged (saying that displacement currents can be neglected). Estimation of the frequency spectra has not been done, but frequencies above $\sim$ 300 kHz are significantly damped by the receiver instrumentation. Hence, in most cases, we believe the quasi-static approximation is valid.

For central-loop configurations, the inversion is normally performed on log-data because the inverse problem is more linear in log data-space. However, because the signal of the on-time gates has alternating sign, the inversion needs to be in the linear-data space, making the inversion convergence slower. Typically, $\sim$ 20% more iterations are needed compared with running the inversion in log-data space.

Conclusion

A system modelling technique has been developed, which combined with primary field-free TEM data improves the model parameter resolution in the near-surface. In this system, modelling the transmitter waveform and receiver filters are combined into a single SR, which we convolve with a step response. This allows us to calculate the forward response for all times – also during the transmitter ramp-down. We have compared a measured SkyTEM SR against an explicit calculation of the SR and validated the SR-modelling at the Danish TEM test site.

As expected, inclusion of on-time gates mainly improves the resolution in the upper $\sim$ 25m, since the newly gained early gates probe mainly the near-surface. Parameter uncertainty analyses show clear improvements in the resistivity determination in the near-surface when on-time gates are included. The analyses also show that the greatest improvements are obtained for thin, high-resistivity layers, where layer boundaries become better defined and estimated resistivities are much closer to the true resistivities. For a field example, we demonstrated that the on-time data can be modelled and fitted well, and we obtain enhanced resolution/changes in the near surface, by including the on-time data both for the conductive and resistive structures. The enhanced resolution comes at no extra cost during surveying and data inversion.

Acknowledgements

We wish to acknowledge Innovation Fund Denmark for funding the Airtech4Water project (project no. 082-2013-3) and rOpen (no. 6150-00006) under which this research was conducted, and University of Wyoming, U.S., for supporting the collection of the field data.

Disclosure statement

No potential conflict of interest was reported by the authors.

Funding

This work was supported by WATEC, Aarhus University Centre for Water Technology; Innovation Fund Denmark: [Grant Number Airtech4Water, project no. 082-2013-3,rOPEN, Procect no. 6150-00006].

ORCID

Esben Auken http://orcid.org/0000-0002-5397-4832
Kristoffer Rønne Andersen http://orcid.org/0000-0001-6204-3522
Anders Vest Christiansen http://orcid.org/0000-0001-5829-2913

References

Andersen, K.R., N.S. Nyboe, C. Kirkegaard, E. Auken, and A.V. Christiansen. 2015. A system response convolution routine for improved near surface sensitivity in SkyTEM Data. *EAGE First European Airborne Electromagnetics Conference*, Tu AEM 07.

Auken, E., T. Boesen, and A.V. Christiansen. 2017. A review of airborne electromagnetic methods with focus on geotechnical and hydrological applications from 2007 to 2017. *Advances in Geophysics* 58: 47–93.

Auken, E., and A.V. Christiansen. 2004. Layered and laterally constrained 2D inversion of resistivity data. *Geophysics* 69: 752–61.

Auken, E., A.V. Christiansen, G. Fiandaca, C. Schamper, A.A. Behroozmand, A. Binley, E. Nielsen, et al. 2015. An overview of a highly versatile forward and stable inverse algorithm for airborne, ground-based and borehole electromagnetic and electric data. *Exploration Geophysics* 46: 223–35.

Balch, S.J., W.P. Boyko, and N.R. Paterson. 2003. The AeroTEM airborne electromagnetic system. *The Leading Edge* 22: 562–66.

Balch, S.J., W.P. Boyko, and N.R. Paterson. 2007. The AeroTEM airborne electromagnetic system. *The Leading Edge*, 562–6.

Effersø, F. 2014. SkyTEM: a versatile HELITEM system: Presented at the Annual Meeting of Association of Exploration Geophysicists. *AEG*.

Everett, M.E. 2012. Theoretical developments in electromagnetic induction geophysics with selected applications in the near surface. *Surveys in Geophysics* 33: 29–63.

Foged, N., E. Auken, A.V. Christiansen, and K.I. Sørensen. 2013. Test site calibration and validation of airborne and ground based TEM systems. *Geophysics* 78: E95–E106.

Forsythe, G.E., M.A. Malcolm, and C.B. Moler. 1977. Interpolation (chapter 4), Numerical integration (chapter 5). In *Computer methods for mathematical computations*, Prentice-Hall

series in automatic computation, 63–105. Englewood Cliffs, NJ: Prentice-Hall, Inc.
HydroGeophysics Group, Aarhus University, Denmark. 2017. SkyTEM Reynolds Creek. Repport 09-02-2017.
Johansen, H.K., and K.I. Sørensen. 1979. Fast Hankel transforms. *Geophysical Prospecting* 27: 876–901.
Kirkegaard, C., K. Andersen, T. Boesen, V. Christiansen, E. Auken, and G. Fiandaca. 2012. Utilizing massively parallel co-processors in the AarhusInv 1D forward and inverse AEM modelling code. *ASEG-PESA*.
Kirkegaard, C., and E. Auken. 2015. A parallel, scalable and memory efficient inversion code for very large-scale airborne electromagnetics surveys. *Geophysical Prospecting* 63: 495–507.
Kirkegaard, C., N. Foged, E. Auken, A.V. Christiansen, and K.I. Sørensen. 2012. On the value of including x-component data in 1D modeling of electromagnetic data from helicopterborne time domain systems in horizontally layered environments. *Journal of Applied Geophysics* 84: 61–9.
Knight, J.H., and A.P. Raiche. 1982. Transient electromagnetic calculations using the Gaver-Stehfest inverse Laplace transform method. *Geophysics* 47: 47–50.
Lane, R., A.G. Green, C. Golding, M. Owers, P. Pik, C. Plunkett, D. Sattel, and B. Thorn. 2000. An example of 3D conductivity mapping using the TEMPEST airborne electromagnetic system. *Exploration Geophysics* 31: 162–72.
Legault, J., A. Prikhodko, D.J. Dodds, J.C. Macnae, and G.A. Oldenborger. 2012. Results of recent VTEM helicopter system development testing over the Spiritwood Valley Aquifer, Manitoba. *SAGEEP, Society of Exploration Geophysicists* 1: 1–17.
Macnae, J., and B. Milkereit. 2007. Developments in broadband airborne electromagnetics in the past decade. *Proceedings of the 5th International Conference on Mineral Exploration*.
Nyboe, N.S., and S.S. Mai. 2017. Recent advances in Skytem receiver system technologies. *EAGE 2nd European Airborne Electromagnetics Conference*.
Raiche, A. 1998. Modelling the time-domain response of AEM systems. *Exploration Geophysics* 29: 103–6.
Schamper, C., E. Auken, and K.I. Sørensen. 2014. Coil response inversion for very early time modelling of helicopterborne time-domain electromagnetic data and mapping of near-surface geological layers. *Geophysical Prospecting* 62: 658–74. doi:10.1111/365-2478.12104.
Seyfried, M., K. Lohse, D. Marks, G. Flerchinger, F. Pierson, and W. Steven Holbrook. 2018. Reynolds creek experimental watershed and critical zone observatory. *Vadose Zone Journal* 17. doi:10.2136/vzj2018.07.0129
Smith, R.S. 2001. On removing the primary field from fixed-wing time-domain airborne electromagnetic data: some consequences for quantitative modelling, estimating bird position and detecting perfect conductors. *Geophysical Prospecting* 49: 405–16.
Sørensen, K.I., and E. Auken. 2004. SkyTEM - a new high-resolution helicopter transient electromagnetic system. *Exploration Geophysics* 35: 194–9.
Spies, B.R. 1989. Depth of investigation in electromagnetic sounding methods. *Geophysics* 54: 872–88.
Tarantola, A., and B. Valette. 1982. Generalized nonlinear inverse problems solved using the least squares criterion. *Reviews of Geophysics* 20: 219–32.
Witherly, K.E., R.J. Irvine, and E. Morrison. 2004. The Geotech VTEM time domain helicopter EM system. *ASEG Extended Abstracts* 2004: 1–4.
Yin, C., R. Smith, G. Hodges, and P. Annan. 2008. Modeling results of on-and off-time B and dB/dt for time-domain airborne EM systems. *70th EAGE Conference and Exhibition incorporating SPE EUROPEC 2008*.

Appendix A: adaptive sampling

The algorithm used for the adaptive sampling is shown in Figure A1. A sketch of the method is shown in Figure A2, We define samplings with 6, 12, 24, 48, and 96 points per decade. Initially the convolution is calculated for 6 points per decade. If a point deviates by more than $C = 10\%$ from a linear interpolation between the two neighbours, we calculate two points in-between the 3 existing points. These points are now spaced at 12 points per decade. The linear interpolation is calculated in logarithmic time and linear response, but can be done in any preferred way. We choose log time and linear response to match the way we integrate over the time gates of the system. After cycling through all points at the 6 points per decade level, we continue to 12 points per decade and perform a refinement wherever necessary. The process continues until 96 points per decade have been reached. The C factor is determined imperially and results in an accuracy better than 1% after convolution.

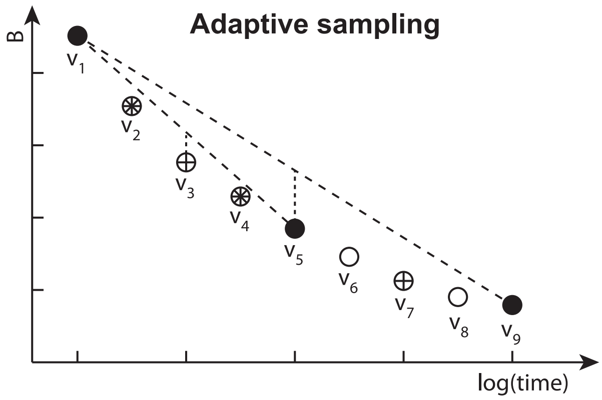

Figure A2. A simple sketch of the adaptive sampling method used on nine points. First, the coarsest sampling is calculated. These are all the black dots. Because v_5 deviates by more than a factor C from a straight line between v_1 and v_9 we evaluate the intermediate points v_3 and v_7. We continue searching for deviations and find that v_3 deviates from the straight line between v_1 and v_5. Hence, we evaluate v_2 and v_4. This is our finest sampling and the refinement process stops.

Appendix B: calculating the system response

To calculate h_{system} and S_0 one can use the time-domain expressions given for first and second order filters relevant to our specific setup and the measured waveform.

The most important filters are the first order Butterworth filter, which is

$$h_1(t) = \omega \exp(-\omega t), \quad t \geq 0, \tag{B1}$$

and the second order critically damped filter which is

$$h_2(t) = \omega^2 t \exp(-\omega t), \quad t \geq 0. \tag{B2}$$

In the present case $h_{system} = h1 * h2$ where the cut-off frequencies are 300 kHz and 210 kHz, respectively. For this filter combination, one can calculate h_{system} analytically. However, this cannot be done for a more general filter configuration. We therefore evaluate the integral numerically and use a fine temporal sampling. The convolution is given by

$$h_{system}(t) = \int_0^t h_1(t-s) h_2(s) ds. \tag{B3}$$

The waveform is often measured using a fast induction coil, which measures dI/dt. From these data we evaluate d^2I/dt^2 and make the convolution with the sampled h_{system}. This is also done numerically and can be done in several ways in practice. A simple way is the following: Assume that d^2I/dt^2 is known at times $t_i, i \in [1, N]$ with values v_i. To calculate $S_0(t) = (d^2I/dt^2) * h_{system}$, we evaluate $h_{systems}$ at times $t'_i = t - t_i$, multiply these values by v_i and use simple trapezoidal integration.

One can check the accuracy of the system response calculation by doing the integral of it. Consider a transmitter waveform. By Fubini's theorem the integral of the system response over all time can be written as

$$\begin{aligned} \int_{-\infty}^{\infty} S' dt &= \int_{-\infty}^{\infty} \frac{d^2I}{dt^2} dt \cdot \int_{-\infty}^{\infty} h_{system} dt \\ &= \left[\frac{dI}{dt}\right]_{-\infty}^{\infty} \cdot \int_{-\infty}^{\infty} h_{system} dt, \end{aligned} \tag{B4}$$

which is zero, since the waveform always starts and ends with a zero slope. Even slight deviations from the zero integral leads to an erroneous calculation of the measured signal.

Algorithm for an adaptive sampling of F(t)

Define levels of time sampling

$$T_1 \subset T_2 \subset \cdots \subset T_N = [t_i, \qquad i = 1, .., n]$$

,

a refinement limit C, and let p be the interpolation factor.

Set $J = 1$ and calculate $F(t_i), t_i \in T_j$.

while $J < N$ **do**

  for $t_i \in T_j$ where $F(t_i)$ is calculated **do**

    If $\frac{|p(F(t_{k,k\neq i})) - F(t_i)|}{|F(t_i)|} > C$ **then**

      Calculate $F(t), t \in T_{j+i}$ and $t_{i-1} < t < t_{i+1}$

    end if

  end for

end while

Figure A1. Algorithm for an adaptive sampling of $F(t)$.